Kasetsart J. (Nat. Sci.) 49 : 451 - 464 (2015)

Extremum-Seeking Gain-Scheduled Adaptive Input Shaping Applied to Flexible-Link Robot

Withit Chatlatanagulchai[1,*], Sermsak Chotana[1] and Chonlawit Prutthapong[2]

ABSTRACT

Input shaping was used to design a finite impulse response (FIR) prefilter. This filter, when convoluted with a reference input, produces a shaped reference input that avoids resonance, resulting in significantly less residual vibration. A flexible system that follows this shaped reference input is able to move from point to point faster due to less settling time. The problem with traditional input shaping is that the filter requires knowledge of the system's natural frequencies and damping ratios and hence its performance deteriorates when the system is time varying. This paper proposed a novel adaptive input shaping algorithm. The system's natural frequencies and damping ratios were gain-scheduled based on system-measured states and were simultaneously adjusted by extremum seeking for minimum residual vibration. The proposed algorithm was applied to the point-to-point movement of a one-link, flexible-link robot manipulator whose payload varied with time. The experimental results confirmed the effectiveness of the proposed algorithm, compared with the unadaptive case.

Keywords: adaptive input shaping, extremum seeking, gain scheduling, flexible link robot

INTRODUCTION

Input shaping was proposed by Singer and Seering (1990), based on the posicast control idea of Smith (1957), to reduce residual vibration from point-to-point movement of lightly damped systems. The technique uses the idea of having two impulse responses cancel each other for zero vibration. If the first impulse is applied at time zero, the unknowns are then the time and magnitude of the second impulse. With knowledge of the natural frequency and damping ratio of the system, the unknowns can be found in closed form by setting the impulse responses to zero. The train of two impulses can be put in a finite impulse response (FIR) filter format. The filter will then be placed after the reference input to create a shaped reference input that will avoid exciting the system's vibratory modes. For system with *n* modes, *n* FIR filters are required.

However knowledge of the natural frequency and damping ratio of the system may be inaccurate due to imperfect system identification, a time-varying system and external disturbance among other factors, causing performance deterioration of the input shaper (Singer and Seering, 1990).

One way to abate the problem is that, instead of two, more impulses are added to the impulse train to provide robustness against the

1 Department of Mechanical Engineering, Faculty of Engineering, Kasetsart University, Bangkok 10900, Thailand.

2 Julajomklao Navy Dockyard, The Royal Thai Naval Dockyard Headquarter, Royal Thai Navy, Samut Prakan 10290, Thailand.

* Corresponding author, e-mail: fengwtc@ku.ac.th

Received date : 10/01/14 Accepted date : 15/03/15

natural frequency and damping ratio variations (Vaughan *et al*., 2008). These additional impulses are found from setting the higher-order derivatives of the impulse responses to zero. The problem with using more impulses is that the shaped reference input is slower, resulting in slower point-to-point movement (Singer and Seering, 1990).

Adaptive schemes are discussed below and can be divided into two groups: 1) an indirect adaptive scheme, where the natural frequencies and damping ratios of the system are identified in real time and used in input shaping filter design; and 2) a direct adaptive scheme, where the input shaping filter is designed directly from real-time adaptive algorithms.

Reported studies on indirect adaptive schemes include Pereira *et al*. (2012) who used a modified algebraic identification method to identify, in real time, the first-mode natural frequency of a single-link, flexible robot manipulator. However, the proposed method requires a simplified plant mathematical model, only identifies a parameter and has no obvious extension to a more complicated system. Stergiopoulos and Tzes (2007) investigated an adaptive input shaping of a nonlinear system. In their work, a simple pendulum's nonlinear equation of motion was used to compute the natural frequency and damping ratio for the adaptive input shaper. The effectiveness of the algorithm then depends on the accuracy of the nonlinear model. In Bodson (1998), the natural frequency and damping ratio of the plant were found by assuming that the plant was represented by a standard second-order lightly damped transfer function. Then, the adaptive inverse technique was used to identify the parameters in real-time. However, the method is restricted to a type of plant, and deviation from the actual plant may disqualify using this method. Tzes and Yurkovich (1993) applied a real-time version of a frequency domain system identification method—called empirical transfer function estimation contained in Ljung (1987)—to estimate plant natural frequencies. The method is based on assumptions of the actual plant being linear and a smooth function of frequencies. Only natural frequencies, not damping ratios, can be adapted with this method. Kozak *et al*. (2004) linearized the nonlinear plant model around operating points. Then, the natural frequencies and damping ratios were obtained from the linearized plant models and used by the input shaper. The effectiveness of the algorithm again depends on the accuracy of the nonlinear model.

Reported studies on direct adaptive schemes include Cole and Wongratanaphisan (2013) who designed a full-order FIR filter, whose coefficients were obtained from a zero residual vibration orthogonality condition. The FIR filter is adapted in real time when new measurements become available using a recursive least-square algorithm. The measurements are those of the shaped reference input and the vibratory state such as a strain gauge signal. The proposed method requires the persistent excitation of the inputs and is computationally expensive. Park *et al*. (2006) used two conventional numerical optimization methods—the golden section search and the secant methods—to directly adjust the impulse magnitude and timing of the input shaper to minimize a vibratory magnitude measure. In order to perform the search, the method requires iterative movement of the system and, therefore, is suitable only for systems such as industrial robots that have has repetitive maneuvers. Cutforth and Pao (2004) used a similar technique to that of Park *et al*. (2006) but instead used the percent vibration, introduced by Rhim and Book (2001), as the vibratory magnitude measure. The modified algorithm does not require repetitive movement, but the plant must be linear in order to compute the percent vibration. Rhim and Book (2004) proposed an adaptive scheme similar to that of Cole and Wongratanaphisan (2013). The scheme is based on the idea that the flexible system and the input shaper can be commuted, which requires that the system be linear.

In this paper, a novel adaptive input

shaping algorithm—the so-called extremum-seeking gain-scheduled input shaping (EGI)—is presented. The system's natural frequencies and damping ratios are gain-scheduled based on system-measured states and are simultaneously adjusted by extremum seeking (Ariyur and Krstic, 2003; Zhang and Ordonez, 2012) for minimum residual vibration. The proposed algorithm has several advantages: 1) EGI does not require a mathematical model of the plant. The system's natural frequencies and damping ratios are determined off-line and can be obtained from experiments or human experience. The extremum-seeking algorithm will further adjust the system's natural frequencies and damping ratios for minimum residual vibration. Being a model-independent method, EGI can then be naturally applied to more complicated or nonlinear systems; 2) EGI adapts multiple parameters. The system's natural frequencies and damping ratios of all vibratory modes can be simultaneously adapted by the extremum-seeking algorithm for minimum-possible residual vibration; 3) EGI does not require persistent excitation of inputs. The convergence of the method is provided by the extremum-seeking algorithm; 4) EGI can be implemented as transfer functions (for the extremum-seeking part) and a look-up table (for the gain-scheduled part) and; therefore, is low on computational effort; 5) EGI does not require repetitive maneuvers. The extremum-seeking continues to adjust the parameters for minimum vibration even when the gain scheduling is not accurate.

MATERIALS AND METHODS

Input Shaping

Consider the two impulse responses shown in Figure 1. For a one-degree-of-freedom, unforced, under-damped, linear system, the response to an impulse with magnitude $\hat{F}_1$ is given by Equation 1:

$$y(t) = \frac{\hat{F}_1 e^{-\zeta\omega_n(t-t_1)}}{m\omega_n\sqrt{1-\zeta^2}} \sin\sqrt{1-\zeta^2}\,\omega_n(t-t_1) \qquad (1)$$

where y is the response, ζ is the damping ratio, ω_n is the natural frequency, m is the mass, and t_1 is the time the impulse is applied. Another impulse $\hat{F}_2$ can then be designed with appropriate magnitude and timing to obtain perfect cancellation of the two impulse responses (Chatlatanagulchai and Saeheng, 2009; Chatlatanagulchai *et al*. 2009) using the knowledge of ω_n and ζ of the system.

The input shaping method (Singer and Seering, 1990) in its simplest form is shown in Figure 2, where: $\bar{r}$ is the reference input; $\bar{F}_1$ and $\bar{F}_2$ are two normalized impulses applied at time t_1 and t_2, which can be realized as an FIR filter; r is the shaped reference input, which is the convolution between $\bar{r}$ and the input shaping FIR filter; and y is the output of a flexible open-loop or closed-loop system with known natural frequency ω_n and damping ratio ζ.

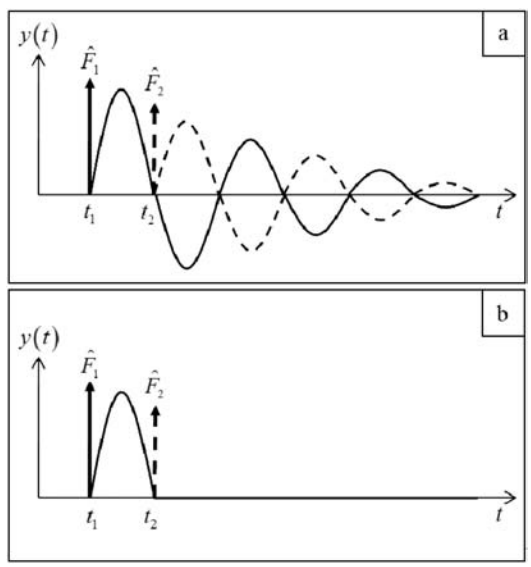

Figure 1 Cancellation of two impulse responses ($\hat{F}_1$ and $\hat{F}_2$) at times t_1 and t_2 : (a) System responses of two impulses; (b) Addition of two impulse responses. y (t) is the response. $\hat{F}_1$ and $\hat{F}_2$ are the magnitudes of the first and second impulses. t_1 and t_2 are the time locations of the first and second impulses.

Perturbation-Based extremum seeking

A diagram of the perturbation-based extremum seeking method is shown in Figure 3. The objective is to find x so that $y = f(x)$ attains its extremum value. As opposed to the gradient method, in which the function f must be known in closed form in order to find the gradient, the extremum seeking method does not need the knowledge of f. The method estimates the local gradient of f by tracking the variation of the function in response to small perturbations.

If $\hat{x}$ is the estimate and x^* is an extremum point of f, it is necessary to show next that the estimation error $\tilde{x} = \hat{x} - x^*$ will approach zero asymptotically with the system in Figure 3. The output value is given by Equation 2:

$$y = f(x) = f\left(\hat{x} + a\sin(\omega t)\right) \approx f(\hat{x}) + \left.\frac{\partial f}{\partial x}\right|_{x=\hat{x}} a\sin(\omega t) \quad (2)$$

where the last approximation is from the first-order Taylor's series of f around $\hat{x}$ The high-pass filter removes the constant $f(\hat{x})$, resulting in Equation 3:

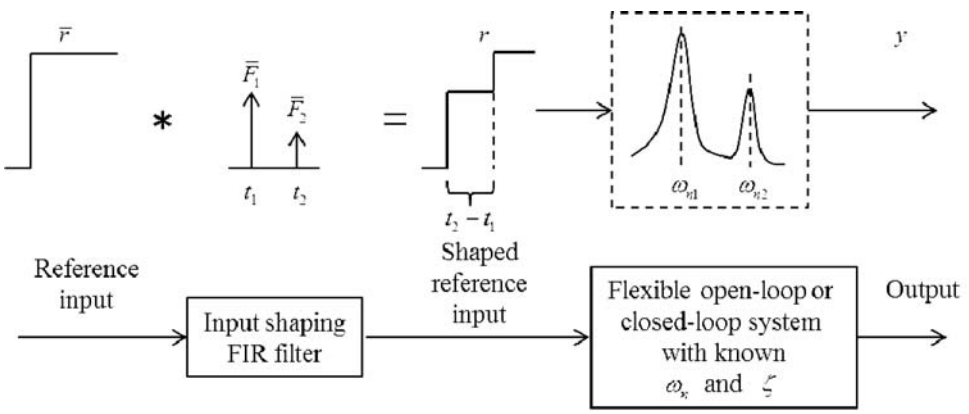

Figure 2 Input shaping for a flexible system, where $\bar{r}$ is the reference input; $\bar{F}_1$ and $\bar{F}_2$ are two normalized impulses applied at time t_1 and t_2, which can be realized as a finite impulse response (FIR) filter; r is the shaped reference input, which is the convolution between $\bar{r}$ and the input shaping FIR filter; and y is the output of a flexible open-loop or closed-loop system with known natural frequency ω_n and damping ratio ζ.

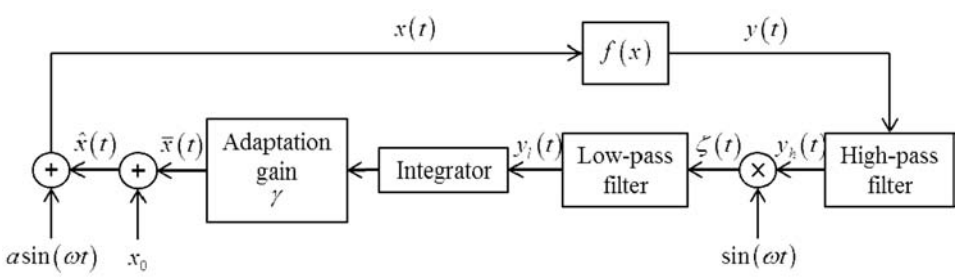

Figure 3 Perturbation-based extremum seeking, where $x(t)$ is the independent signal, $f(x)$ is the function to be minimized, $y(t)$ is the minimized signal, $y_h(t)$ is the signal from the high-pass filter, ω is the designed frequency, $\zeta(t)$ is the signal to the low-pass filter, $y_l(t)$ is the signal from the low-pass filter, γ is the adaptation gain, $\bar{x}(t)$ is the signal after multiplying the adaptation gain, x_0 is the bias signal, $\hat{x}(t)$ is the signal after bias and a is the amplitude of the sine wave.

$$y_h \approx \left.\frac{\partial f}{\partial x}\right|_{x=\hat{x}} a\sin(\omega t) \tag{3}$$

and then, Equation 4:

$$\begin{aligned}\zeta = y_h \sin(\omega t) &\approx \left.\frac{\partial f}{\partial x}\right|_{x=\hat{x}} a\sin^2(\omega t) \\ &= \left.\frac{\partial f}{\partial x}\right|_{x=\hat{x}} \frac{a}{2} - \left.\frac{\partial f}{\partial x}\right|_{x=\hat{x}} \frac{a}{2}\cos(2\omega t)\end{aligned} \tag{4}$$

After the low-pass filter, which removes the cos(2ωt) term, the estimated local gradient is given by Equation 5:

$$y_l \approx \left.\frac{\partial f}{\partial x}\right|_{x=\hat{x}} \frac{a}{2} \tag{5}$$

and the updating law shown in Equation 6:

$$\dot{\hat{x}} = \dot{\bar{x}} = \gamma y_l \tag{6}$$

where x_0 is constant and could be an initial guess of x^* and γ is a negative constant design parameter used as adaptation gain.

Consider the second-order Taylor's series of f around x^*, as shown in Equation 7:

$$\begin{aligned}f(x) &\approx f(x^*) + f'(x^*)(x-x^*) + \frac{1}{2}f''(x^*)(x-x^*)^2 \\ &= f(x^*) + \frac{1}{2}f''(x^*)(x-x^*)^2\end{aligned} \tag{7}$$

where $f'(x^*) = 0$ because $x^*$is an extremum point of f. The local gradient is then given by Equation 8:

$$\left.\frac{\partial f}{\partial x}\right|_{x=\hat{x}} \approx f''(x^*)(\hat{x}-x^*) \tag{8}$$

Because $\dot{\hat{x}} = \dot{\bar{x}}$, using equations, and results in Equation 9:

$$\dot{\tilde{x}} \approx \frac{a\gamma f''(x^*)}{2}\tilde{x} \tag{9}$$

which shows that $\tilde{x}$ will approach zero asymptotically, provided that $a < 0$ when in a maximization problem ($f''(x^*) < 0$) or $a > 0$ when in a minimization problem ($f''(x^*) > 0$)

Flexible-Link robot system

The proposed flexible-link robot hardware used in the experiments is shown in Figure 4. A 30 cm steel ruler is used as the flexible link. An adjustable payload is placed at its tip. An accelerometer is attached at the tip, a strain gauge near the pivot and an optical encoder to measure the DC motor's angle.

A schematic diagram is given in Figure 5, where θ is the motor angle, θ_s is additional angle of the payload as obtained from the strain gauge, $\theta_p = \theta + \theta_s$ is the payload angle, and a_p is the payload acceleration, measured from the accelerometer.

Figure 6 shows the real-time control system setup. A National Instrument (National Instruments; Austin, TX, USA) system was used. Note that u is the control input sent to the motor driver.

Because the input shaping needs the natural frequencies and damping ratios of the

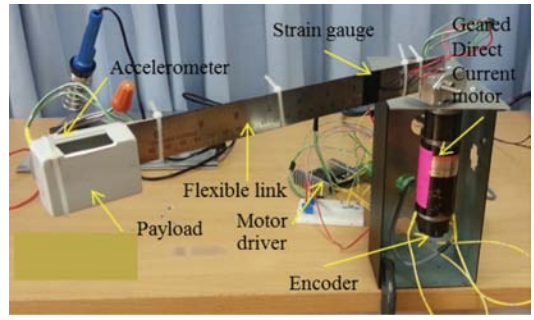

Figure 4 The flexible-link robot hardware used in our experiments.

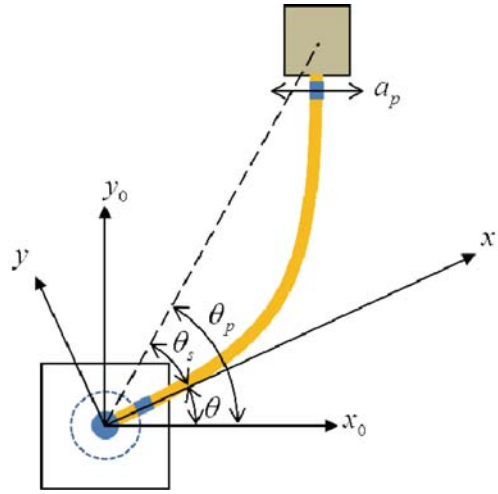

Figure 5 Schematic diagram of the flexible-link robot.

system, a closed-loop experiment was performed where there is no payload by having the reference motor angle θ_r be a sweep square wave with 20° amplitude and sweeping frequencies from 0.1 to 0.5 Hz in 60 s. A PI controller with $k_p = 0.1$ and $k_i = 0.05$ was used. Figure 7 contains the periodogram of a_p, showing the first-mode natural frequency of

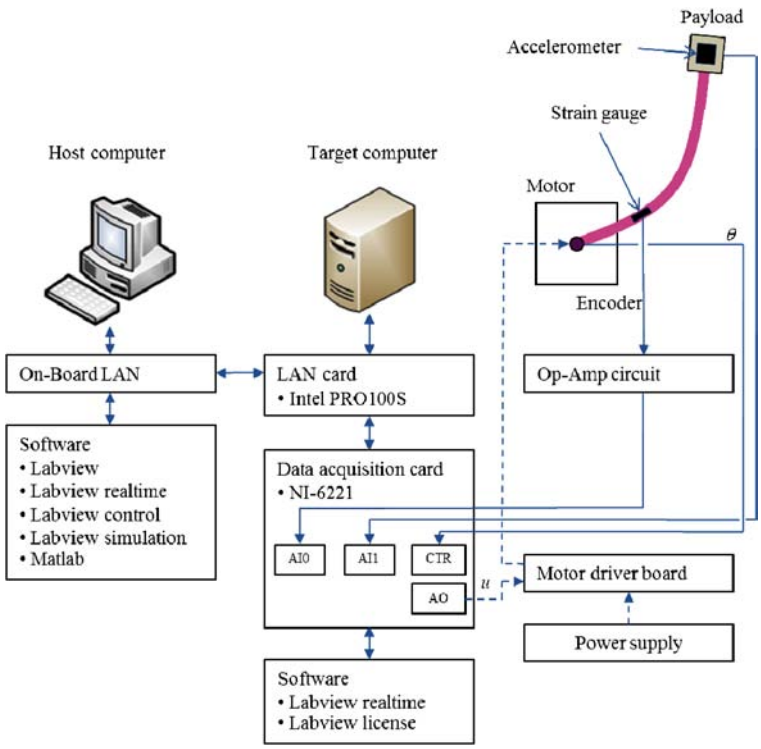

Figure 6 Schematic diagram of real-time control system. u is the command input to the motor driver board. θ is the motor angular position.

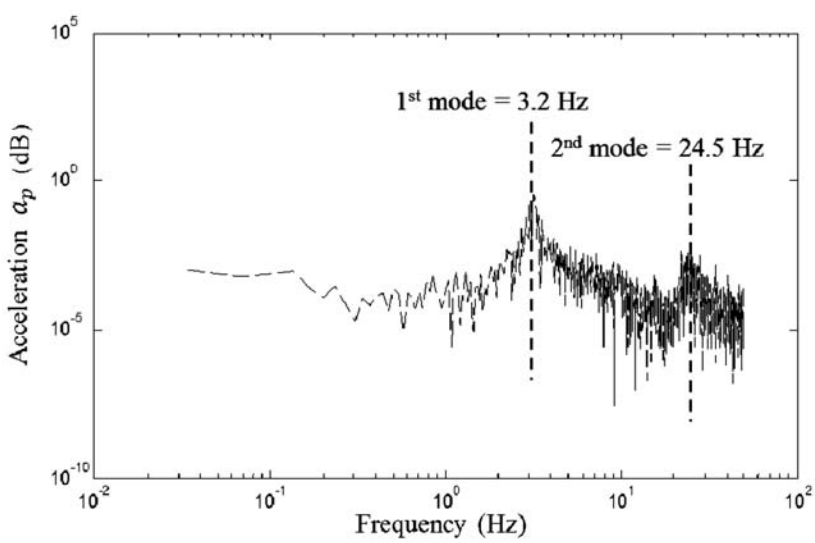

Figure 7 Periodogram of acceleration showing the first and second modes.

3.2 Hz and the second-mode natural frequency of 24.5 Hz.

The first-mode damping ratio was obtained by fixing one end of the flexible arm, giving initial angular displacement, then releasing and measuring θ_s with the strain gauge. Figure 8 shows the time in seconds versus the angle θ_s in volts, which is the unit of the strain gauge signal. From the logarithmic decrements formula, the damping ratio ζ was computed as

$$\delta = \frac{1}{n}\ln\frac{x_0}{x_n} = \frac{1}{5}\ln\frac{0.00532}{0.002891} = \frac{2\pi\zeta}{\sqrt{1-\zeta}}$$

$$\zeta = 0.0192$$

This damping ratio was used for both the first mode and second mode.

Unadaptive input shaping

Figure 9 contains a diagram of the unadaptive input shaping, where F is the input shaper, C is the PI controller, P is the flexible arm, $\bar{\theta}_r$ is the motor reference angle, θ_r is the motor shaped reference angle, and e is the motor angle tracking error. Other variables are as previously defined.

The input shaper F uses the closed-loop natural frequencies and damping ratios as design parameters, which are unchanged in the unadaptive case.

With the same PI controller as that of the previous section, and P is defined by Equation 10:

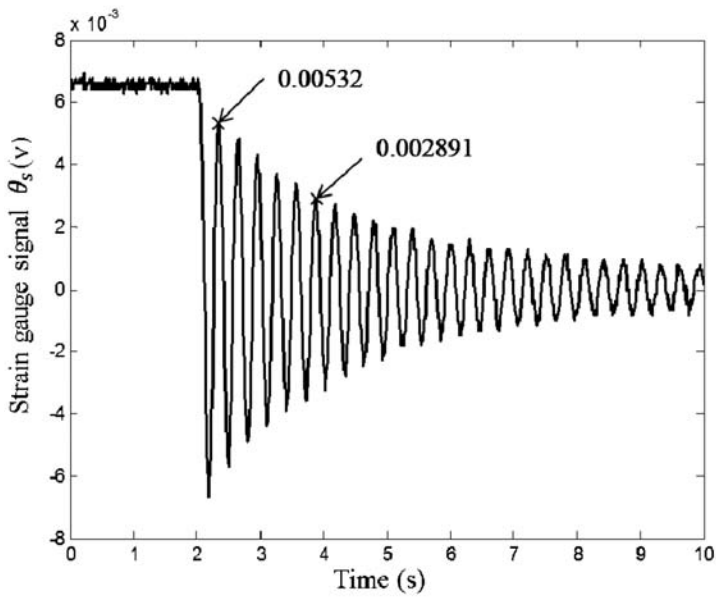

Figure 8 Strain gauge signal to determine the damping ratio.

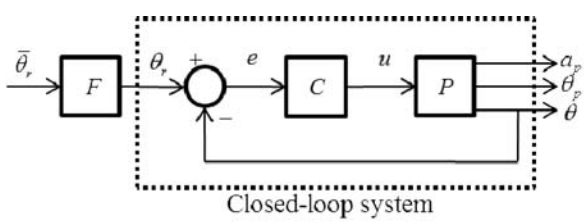

Figure 9 Diagram of the unadaptive input shaping, where $\bar{\theta}_r$ is the unshaped reference, θ_r is the shaped reference, e is the tracking error, u is the control effort, a_p is the payload acceleration, θ_p is the payload angular position and θ is the motor angular position. F is the pre-filter; C is the feedback controller and P is the plant.

$$P = \left(\frac{\bar{\omega}_{n1}^2}{s^2 + 2\bar{\zeta}_1 \bar{\omega}_{n1} s + \bar{\omega}_{n1}^2} \right) \left(\frac{\bar{\omega}_{n2}^2}{s^2 + 2\bar{\zeta}_2 \bar{\omega}_{n2} s + \bar{\omega}_{n2}^2} \right) \quad (10)$$

where $\bar{\omega}_{n1}$, $\bar{\omega}_{n2}$, $\bar{\zeta}_1$, and $\bar{\zeta}_2$ are those of the previous section, the closed-loop natural frequencies and damping ratios of the first and second modes can then be computed as ω_{n1} = 21.105 rad.s^{-1}, ω_{n2} = 153.804 rad.s^{-1}, ζ_1 = 0.017, and ζ_2 = 0.019.

The input shaper F can be written as an FIR filter using Equation 11:

$$F(z) = F_1(z) F_2(z) \quad (11)$$

where $F_i(z) = \left(\bar{F}_1 + \bar{F}_2 z^{-\frac{t_2}{t_s}} + \bar{F}_3 z^{-\frac{t_3}{t_s}} \right)$ belongs to the ith mode, with

$$\bar{F}_1 = 1/(1 + 2K + K^2)$$
$$\bar{F}_2 = 2K/(1 + 2K + K^2)$$
$$\bar{F}_3 = K^2/(1 + 2K + K^2)$$
$$K = e^{\frac{-\zeta\pi}{\sqrt{1-\zeta^2}}}$$
$$t_2 = \frac{\pi}{\omega_n \sqrt{1-\zeta^2}}$$
$$t_3 = \frac{2\pi}{\omega_n \sqrt{1-\zeta^2}}$$

where t_s is the sampling time, and z is the z-transform operator.

The payload acceleration must be put in a quantifiable form to be able to be reduced which requires the design of a quantity as shown by Equation 12:

$$\hat{a}_p = \int |a_p| \, dt \quad (12)$$

where the integration is taken over the preceding movement of the flexible link.

Extremum-Seeking gain-scheduled input shaping system

When the payload changes, the performance degradation found in the unadaptive case is because the actual system's natural frequencies and damping ratios change with the payload but the unadaptive input shaping was designed based on fixed natural frequencies and damping ratios. Here, an adaptive system is presented to adjust these design parameters on-line. The system, shown in Figure 10, consists of four parts: the input shaper, the closed-loop motor controller, the extremum seeking and the gain scheduler. The outputs from the extremum

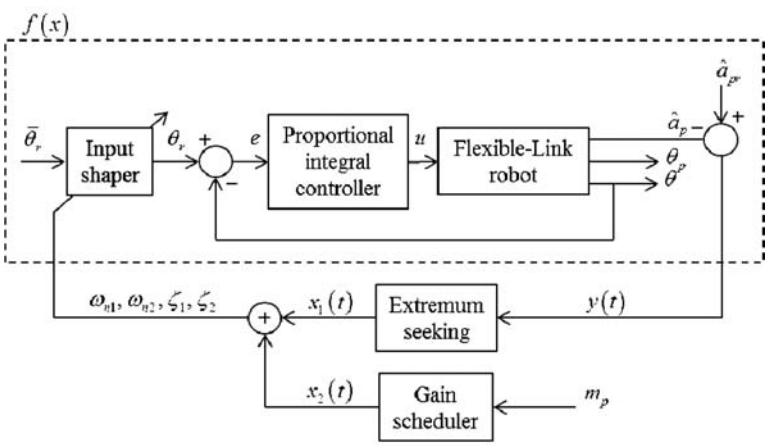

Figure 10 Extremum-seeking, gain-scheduled input shaping system, where $\bar{\theta}_r$ is the unshaped reference, θ_r is the shaped reference, e is the tracking error, u is the control effort, $\hat{a}_p$ is the quantified payload acceleration, $\hat{a}_{pr}$ is the reference signal for $\hat{a}_p$, θ_p is the payload angular position and θ is the motor angular position, y is the signal to be minimized, x_1 is the output of the extremum seeking algorithm, m_p is the payload mass, x_1 is the output of the gain scheduler, ω_{n1} and ω_{n2} are the first and second natural frequencies and ζ_1 and ζ_1 are the first and second damping ratios and $f(x)$ is the minimized function.

seeking and the gain scheduler are added together and are supplied to the input shaper in adapting its parameters.

The input shaper receives an unshaped motor reference trajectory and outputs the shaped motor reference trajectory. The information used by the input shaper is the first-mode and second-mode natural frequencies and damping ratios of the closed-loop motor controller system. The input shaper here has the same structure as that of the unadaptive input shaper.

The closed-loop motor controller system comprises the PI controller and the flexible-link robot manipulator. The motor angular position is fed back to the PI controller, whose gains are the same as those of the previous section.

The extremum seeking system tries to minimize $y = \hat{a}_{pr} - \hat{a}_p$, where $\hat{a}_{pr}$ is the reference for $\hat{a}_p$ and is set to zero throughout the experiments. The outputs from the extremum seeking are $x_1 = \{\Delta\omega_{n1}, \Delta\omega_{n2}, \Delta\zeta_1, \Delta\zeta_2\}$, which are the changes in the natural frequencies and damping ratios of both modes. Recall that x_1 will be found by the extremum seeking to minimize y.

For the case when the gain-scheduler is not used, the following design parameters are used for the extremum seeking: $\omega = 2$ *rad.s*$^{-1}$; a high-pass filter $s / (s + h)$, where $h = 0.5$; a low-pass filter $l / (s + l)$, where $l = 1$; $a_{\omega_{n1}} = 1$, $a_{\zeta 1} = 0.001$, $a_{\omega_{n2}} = 1$, $a_{\zeta 2} = 0.0015$, are amplitudes of the sine functions in the algorithm; $\gamma_{\omega_{n1}} = -100$, $\gamma_{\zeta 1} = -0.07$, $\gamma_{\omega_{n2}} = -1{,}000$, $\gamma_{\zeta 2} = -0.1$, are the adaptation gains.

For the case when the gain-scheduler is used, the following design parameters are used for the extremum seeking: $a_{\omega_{n1}} = 0.1$, $a_{\zeta 1} = 0.0001$, $a_{\omega_{n2}} = 0.1$, $a_{\zeta 2} = 0.00015$, are amplitudes of the sine functions in the algorithm; $\gamma_{\omega_{n1}} = -10$, $\gamma_{\zeta 1} = -0.007$, $\gamma_{\omega_{n2}} = -100$, $\gamma_{\zeta 2} = -0.01$, are the adaptation gains. Other design parameters are the same as those when the gain-scheduler is not used. Note that because the gain scheduler supplies the nominal values of the natural frequencies and damping ratios, the extremum seeking is less involved and its gains are reduced.

The gain scheduler receives the payload mass m_p as input. In an actual industrial system, the payload mass can be measured by installing a force sensor. In this case, there are four levels of payload using small silver coins: 0 coins; 3 coins; 6 coins and 9 coins.

Table 1 contains the closed-loop natural frequencies and damping ratios with various payloads. These nominal values, $x_2 = \{\bar{\omega}_{n1}, \bar{\omega}_{n2}, \bar{\zeta}_1, \bar{\zeta}_2\}$, were obtained from repeating the experiment in the previous section with the altered amount of payload and were used by the gain scheduler.

RESULTS

The experiments with the flexible-link robot system shown in Figure 4 used as the objective having the payload track a square-wave reference, of 20° amplitude and 30 s period, as closely as possible, with minimum settling time

Table 1 Closed-loop natural frequencies and damping ratios, obtained from experiments, with different coin payloads.

	0 coins	3 coins	6 coins	9 coins
$\bar{\omega}_{n1}\left(\text{rad.s}^{-1}\right)$	21	18	15	12
$\bar{\zeta}_1$	0.017	0.015	0.012	0.010
$\bar{\omega}_{n2}\left(\text{rad.s}^{-1}\right)$	153	130	100	70
$\bar{\zeta}_2$	0.019	0.016	0.013	0.010

$\bar{\omega}_{n1}$ and $\bar{\omega}_{n2}$ are the first and second natural frequencies. $\bar{\zeta}_1$ and $\bar{\zeta}_2$ are the first and second damping ratios.

and residual vibration while the small silver coin payload changed from 0 to 9 to 3 to 6 then back to 9 coins during maneuvering.

Four cases were compared experimentally: 1) without input shaping (WI); 2) with unadaptive input shaping (UI); 3) extremum seeking together with input shaping (EI) and 4) extremum seeking with gain scheduling and input shaping (EGI).

Figure 11 contains the comparative results between WI and EGI—the worst case versus the best case. The experiment had no coin payload. Figure 11a and Figure 11b are motor angular positions θ and their references in the WI and EGI cases, respectively. The dashed lines are references, and the solid lines are actual positions. Figure 11c and Figure 11d are payload angular positions θ_p and their references in the WI and EGI cases, respectively. Figure 11e and Figure 11f are payload accelerations a_p in the WI and EGI cases, respectively. Figure 11g and Figure 11h are control

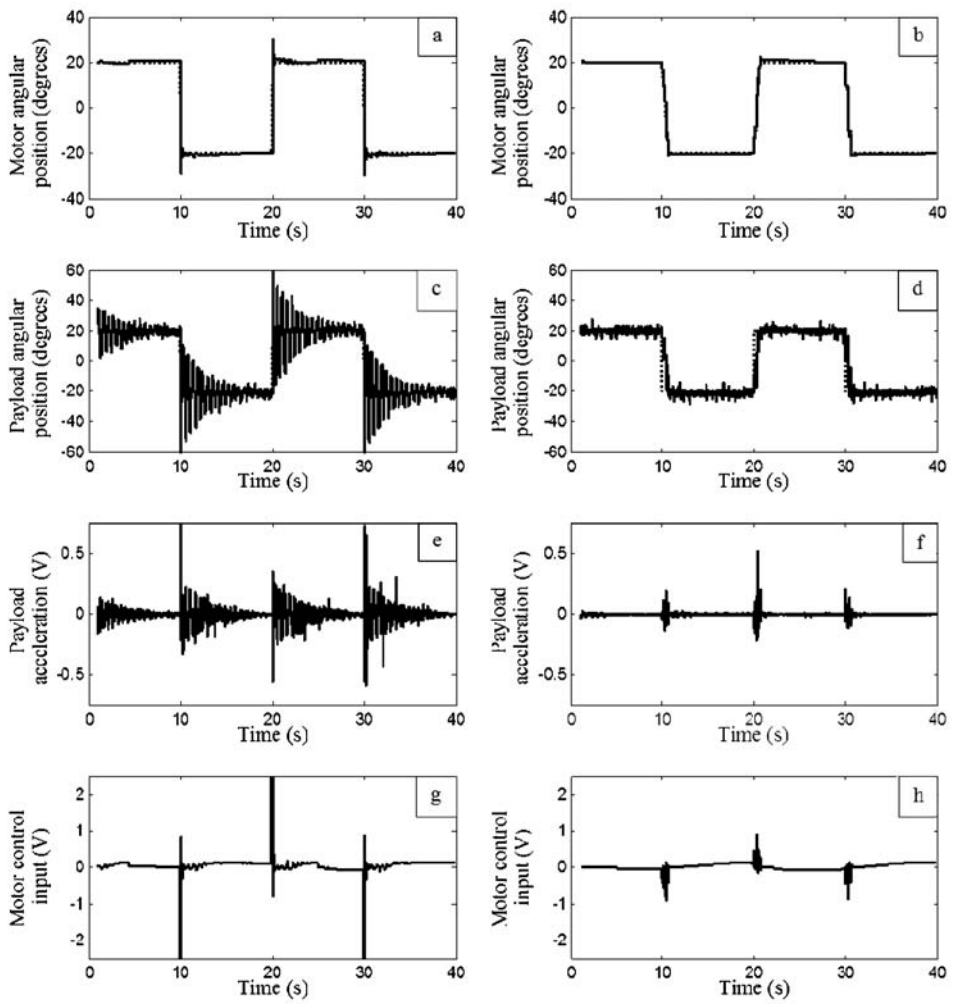

Figure 11 Comparison between cases without input shaping and with extremum-seeking gain-scheduled input shaping (EGI): (a) Motor angular position and its reference (without input shaping); (b) Motor angular position and its reference (EGI); (c) Payload angular position (without input shaping); (d) Payload angular position (EGI); (e) Payload acceleration (without input shaping); (f) Payload acceleration (EGI); (g) Motor control input (without input shaping); (h) Motor control input (EGI).

inputs given to the motor in the WI and EGI cases, respectively. The control saturation is at ± 2.5 V.

Figure 12 compares the accumulated payload vibration $\hat{a}_p$, given in Equation, for all four cases (WI, UI, EI and EGI). Note that the accumulated payload vibration is taken over one movement cycle of the flexible link; therefore, it appears as steps. The input shaper is started with the 0-coin design parameters given in

Table 1. Then, in the UI case, the input shaper keeps the same design parameters throughout the experiment, whereas, in the EI and EGI cases, the design parameters are changed based on the algorithms.

Figure 13 concentrates on the accumulated payload vibration $\hat{a}_p$ of the EGI case, which shows the merit of having the extremum seeking further adjust the design parameters given by the gain scheduler.

Figure 14 contains a comparison of the adaptations of the design parameters between the EI and EGI cases.

DISCUSSION

In Figure 11a and Figure 11b, with the PI controller, the motor is able to follow its reference quite well in both cases. Note that in EGI, the reference is more tapered due to convolution between the square wave and the train of impulses in the input shaper.

In Figure 11c and Figure 11d, the 10% settling time in the WI case is 10 s while in the EGI case, it is 0.5 s. The outstanding transient performance of the EGI is due mainly to nearly zero payload vibration.

In Figure 11e and Figure 11f, it can be seen that WI has a high-level of payload acceleration, while EGI has almost none.

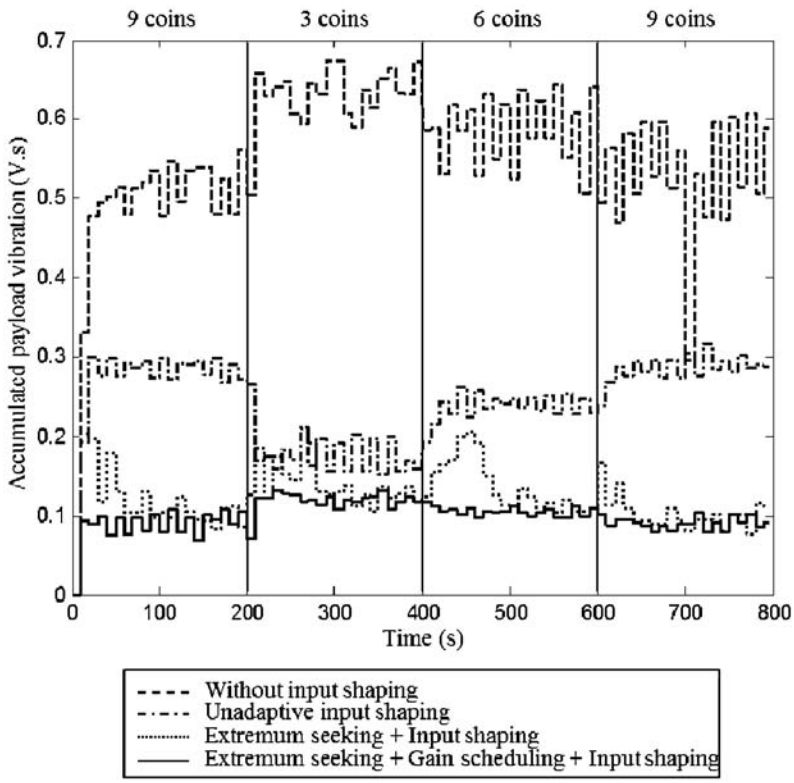

Figure 12 Comparison of accumulated payload vibration among various cases.

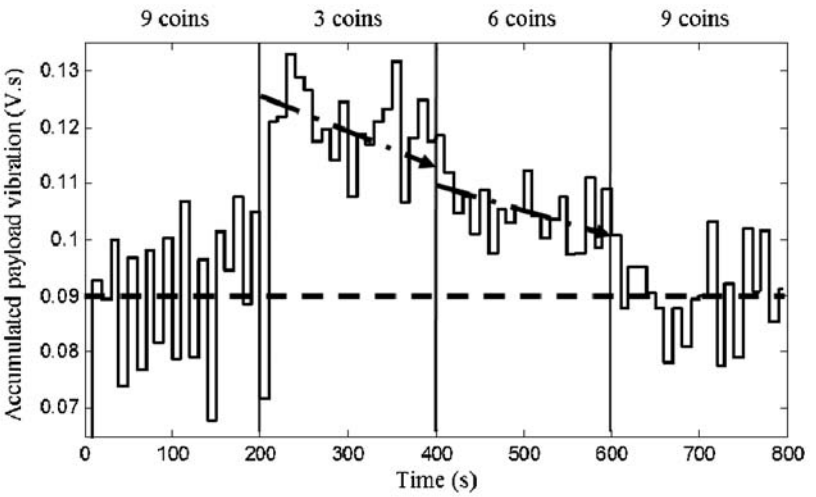

Figure 13 A closer look at the accumulated payload vibration of extremum-seeking gain-scheduled input shaping.

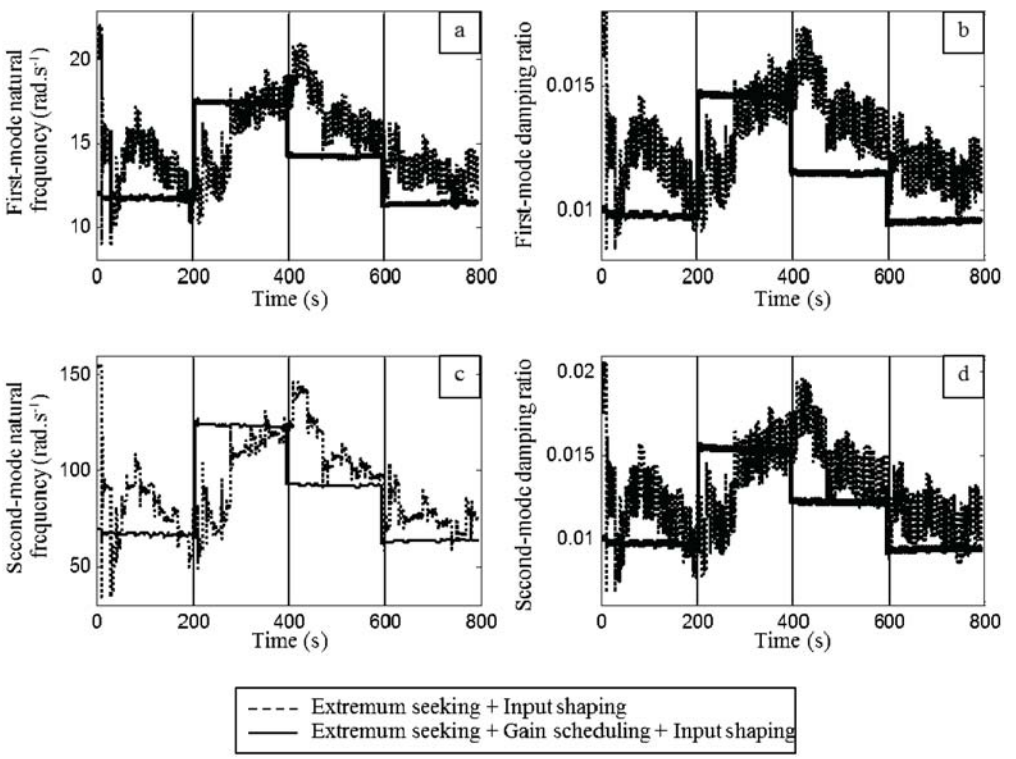

Figure 14 Adaptations of natural frequencies and damping ratios used by the input shaper: (a) First-mode natural frequency; (b) First-mode damping ratio; (c) Second-mode natural frequency; (d) Second-mode damping ratio, a comparison between extremum seeking together with input shaping and extremum-seeking gain-scheduled input shaping cases.

In Figure 11g and Figure 11h, the control saturation is at ± 2.5 V. WI violates this control saturation briefly at points where the reference changes, while EGI has the control input well within the saturation limit.

In Figure 12, in the WI case, when the input shaper is not used, $\hat{a}_p$ ranges from 0.48 to 0.68 V.s. The highest level of payload vibration is with the 3-coin payload, followed by the 6- and 9-coin payloads, respectively, because the lighter the payload, the higher the acceleration. In the UI case, when only the input shaper is used without adaptation, $\hat{a}_p$ ranges from 0.16 to 0.3 V.s. The lowest payload vibration is during the 3-coin payload, followed by the 6- and 9-coin payloads, respectively, because the unadaptive input shaper is designed with the 0-coin design parameters, and so is more favorable to a lighter payload case. In the EI case, when the input shaper is adapted by the extremum seeking algorithm only, $\hat{a}_p$ ranges from 0.1 to 0.2 V.s. At each payload change, it is evident that the extremum seeking starts to adapt the input shaper immediately without having to wait for some repetitive cycles. The vibration continuously lessens after each payload change; however, the adaptation still takes some time before a minimum vibration level is reached. In the EGI case, when the input shaper is adapted by the extremum seeking and gain scheduling algorithms, $\hat{a}_p$ ranges from 0.07 to 0.13 V.s. Although the steady-state payload vibration of the EGI case is comparable to that of the EI case, the transient payload vibration (at each payload change) is much improved because the initial design parameters of the input shaper jump to new and appropriate values as given by the gain scheduler. Note that $\hat{a}_p$ of 0.07 is about the minimum value that can be attained with almost no residual vibration at all.

Figure 13 shows the merit of having the extremum seeking further adjust the design parameters given by the gain scheduler. During the 3- and 6-coin payloads, the payload vibration is in decreasing trends due to the further adaptation provided by the extremum seeking. Note that, during the 9-coin payload, no improvement in vibration is obvious because the payload vibration is already around its minimum value.

In Figure 14, in the EI case, all design parameters gradually adapt to new appropriate values, whereas, in the EGI case, all design parameters are started close to appropriate values by the gain scheduler, resulting in less adaptation required and less transient residual vibration.

CONCLUSION

Unadaptive input shaping uses fixed design parameters, resulting in degrading vibration reduction performance when applied with uncertain and time-varying systems. A new adaptive algorithm using extremum seeking and gain scheduling was proposed. The extremum seeking is a mathematical, model-free, optimization algorithm that locally finds the optimum point by using a perturbing sine-wave signal to approximate the gradient of the cost function. Being a local approximation method, the extremum seeking takes more time and loses its effectiveness when the system's character jumps, as for example with a sudden change in payload. The gain scheduling can then be used to provide a look-up table of initial design parameters suitable for each system character.

The proposed adaptive algorithm proved its effectiveness by being applied to the point-to-point movement of a very flexible-link robot manipulator. The residual vibration was reduced to almost zero even when the payloads were changed during maneuvering.

Future research may concentrate on several aspects. 1) The gain scheduler needs to know the system state (in this case, the payload amount), in order to look up the appropriate design parameters for the input shaper. Even though a physical sensor can be put into the system to measure such state, it might be preferable to develop an algorithm to detect the system state from already measured signal such as that of a

strain gauge or accelerometer. 2) In extremum seeking, all design parameters (natural frequencies and damping ratios of all vibratory modes) are adjusted to minimize one vibration signal in the time domain. It would be worth considering minimizing signals in the frequency domain, so the design parameters can be adjusted for each mode separately.

LITERATURE CITED

Ariyur, K.B. and M. Krstic. 2003. **Real-Time Optimization by Extremum-Seeking Control.** 1st ed. Wiley Interscience. Hoboken, NJ, USA. 236 pp.

Bodson, M. 1998. An adaptive algorithm for the tuning of two input shaping methods. **Automatica** 34: 771–776.

Chatlatanagulchai, W. and K. Saeheng. 2009a. Real-time reference position shaping to reduce vibration in slewing of a very-flexible-joint robot. **IJRET** 6: 51–66.

Chatlatanagulchai, W., T. Srivongsa and P.H. Meckl. 2009b. Reference input shaping to reduce move time of a very flexible one-link manipulator. **Kasetsart J. (Nat. Sci.)** 43: 411–421.

Cole, M.O.T. and T. Wongratanaphisan. 2013. A direct method of adaptive FIR input shaping for motion control with zero residual vibration. **IEEE/ASME Trans. Mechatronics** 18: 316–327.

Cutforth, C.F. and L.Y. Pao. 2004. Adaptive input shaping for maneuvering flexible structures. **Automatica** 40: 685–693.

Kozak, K., I. Ebert-Uphoff and W. Singhose. 2004. Locally linearized dynamic analysis of parallel manipulators and application of input shaping to reduce vibrations. **ASME J. Mechanical Design** 126: 156–168.

Ljung, L. 1987. **System Identification Theory for the User.** 1st ed. Prentice Hall. Upper Saddle River, NJ, USA. 609 pp.

Park, J., P.H. Chang, H.S. Park and E. Lee. 2006. Design of learning input shaping technique for residual vibration suppression in an industrial robot. **IEEE/ASME Trans. Mechatronics** 11: 55–65.

Pereira, E., J.R. Trapero, I.M. Diaz and V. Feliu. 2012. Adaptive input shaping for single-link flexible manipulators using an algebraic identification. **Contr. Eng Pract.** 20: 138–147.

Rhim, S. and W.J. Book. 2001. Noise effect on adaptive command shaping methods for flexible manipulator control. **IEEE Trans. Contr. Syst. Tech.** 9: 84–92.

___. 2004. Adaptive time-delay command shaping filter for flexible manipulator control. **IEEE/ASME Trans. on Mechatronics** 9: 619–626.

Singer, N.C. and W.C. Seering. 1990. Preshaping command inputs to reduce system vibration. **ASME J. Dyn. Syst., Meas. Contr.** 112: 76–82.

Smith, O.J.M. 1957. Posicast control of damped oscillatory systems. **Proc. IRE.** 45: 1249–1255.

Stergiopoulos, J. and A. Tzes. 2007. Adaptive input shaping for nonlinear systems: A case study. **ASME J. Dyn. Syst., Meas. Contr.** 129: 219-223.

Tzes, A. and S. Yurkovich. 1993. An adaptive input shaping control scheme for vibration suppression in slewing flexible structures. **IEEE Trans. Contr. Syst. Tech.** 1: 114–121.

Vaughan, J., A. Yano and W. Singhose. 2008. Comparison of robust input shapers. **J. of Sound Vibration** 315: 797–815.

Zhang, C. and R. Ordonez. 2012. **Extremum-Seeking Control and Applications** (1st ed.). Springer. London, UK. 197 pp.